

# Nucleation and growth of zinc on aluminum from acidic sulfate solution with [BMIM]HSO<sub>4</sub> as additive

Qibo Zhang · Yixin Hua

Received: 26 September 2010/Accepted: 3 March 2011/Published online: 13 March 2011  
© Springer Science+Business Media B.V. 2011

**Abstract** The nucleation and first stages of the growth of zinc on aluminum from acidic sulfate solution in the absence and presence of 1-butyl-3-methylimidazolium hydrogen sulfate-[BMIM]HSO<sub>4</sub> as additive were investigated using cyclic voltammetry, chronoamperometric current-time transients, and scanning electron microscopy techniques. The dimensionless chronoamperometric current-time transients for the zinc electrodeposition on aluminum electrode from the solution free of [BMIM]HSO<sub>4</sub> showed the zinc deposition can be interpreted by a model involving instantaneous nucleation with hemispherical diffusion controlled growth of nuclei. The addition of [BMIM]HSO<sub>4</sub> induced a blocking effect on the zinc electrocrystallization process through its cathodic adsorption on the electrode surface. This effect led to increase the number density of active sites, decrease the nucleation and growth rate of these nuclei, and produce more leveled and fine-grained cathodic deposits without affecting the instantaneous nucleation mechanism. Surface morphology analysis revealed the crystal structure of the zinc deposits formed did not change by the adsorption of [BMIM]HSO<sub>4</sub> at the first stages of deposition.

**Keywords** Zinc electrodeposition · Ionic liquid · Additive · Nucleation and growth · Morphology

## 1 Introduction

Electrodeposition of zinc and its alloys for corrosion-resistance applications has been widely investigated [1–3]. However, over half of the world's zinc is produced from acidic sulfate solutions by electrodeposition [4, 5], which is extremely sensitive to the presence of certain metallic impurities [6–9]. Low levels of these impurities greatly interfere in the deposition process, leading to a decrease in zinc current efficiency and to changes in deposits' morphology [10] and cathodic polarization [11, 12]. To counteract the harmful effects of these metallic impurities and obtain deposits expected, the use of additives in electrolytic baths is inevitable. The quantity of additive required is always considerably small (parts per million), but their action is often specific [13]. Their presence in the electrolyte influences the nucleation and growth behavior and therefore, promotes the formation of smooth and bright coatings. The specific activity of an additive is frequently assumed to be the adsorption of additive molecules onto the cathode surface during electrodeposition, which affects the activation energy [14] and the rate of charge transfer in the electrochemical reaction, and influences the mechanism of electrocrystallization [15] by inducing a change at the initial stages of the electrochemical phase formation process. The study of the initial stages is very helpful to understand the nucleation process and provides important information on growth morphology at the early stages of metal deposition as it seems to be significant in determining the morphology and physicochemical properties of the electrodeposited layer [16]. However, for zinc electrodeposition, the initial stage of zinc electrocrystallization has been little studied. Most of the literature concentrates on the effects of additives on the current efficiency and polarization behavior as well as their effects on deposit

Q. Zhang (✉) · Y. Hua  
Key Lab of Ionic Liquids Metallurgy,  
Faculty of Metallurgical and Energy Engineering,  
Kunming University of Science and Technology,  
Kunming 650093, China  
e-mail: qibozhang@yahoo.com.cn

morphology and crystallographic orientations of the cathode during zinc electrodeposition process. Scant information is available on the effects of additives on the early stage nucleation and growth mechanism of zinc from acidic sulfate solution.

Trejo et al. [17, 18] observed that the addition of polyethoxylated compounds to an acidic chloride bath had a blocking effect on the electrodeposition of zinc at the first stages of the nucleation process and this effect was dependent on the molecular weight of the additive. In addition, the nucleation process was found to be modified in the presence of the additives in the electrolytic bath. Yu et al. [19] investigated the temperature dependence of the electrocrystallization of zinc onto a glassy carbon (GC) electrode using cyclic voltammetry and chronoamperometry measurements and found that increasing the temperature increased the nucleation density and modified the nucleation mechanism of zinc electrodeposits. Higashi et al. [20] has developed zinc hydroxide layer suppression mechanisms for zinc deposition in acid sulfate baths, which has been confirmed by other authors [21, 22]. Sonneveld et al. [23] reported that zinc nucleation from a zincate solution on carbon substrate can be interpreted by a model involving instantaneous nucleation in conjunction with three-dimensional hemispherical growth. Raeissi et al. [24] observed that the nucleation mode is instantaneous when zinc electrodeposition from acidic sulfate bath on the steel substrate at pH = 2, whereas increasing the pH of the plating bath to 4, the nucleation process shifted toward progressive. Alvarez et al. [25] studied the first stages of the zinc electrodeposition process on highly oriented pyrolytic graphite from an acidic sulfate solution with gelatine as additive and demonstrated that the nucleation mode for the zinc electrodeposition was instantaneous in the case of additive-free bath, whereas the nucleation process shifted toward more progressive in the presence of gelatine in the solution.

In the previous report [26], 1-butyl-3-methylimidazolium hydrogen sulfate-[BMIM]HSO<sub>4</sub> and its mixture with gelatine have a pronounced inhibiting effect on Zn<sup>2+</sup> discharge and both are found to be efficient as leveling agents. Therefore, it is interesting to investigate the nucleation and growth mechanism of zinc in the presence of [BMIM]HSO<sub>4</sub>. The aim of this study is to gain further insight into the early stages of zinc electrodeposition process from acidic sulfate solution in the presence of [BMIM]HSO<sub>4</sub> as additive.

## 2 Experimental

The zinc electrolyte concentration of 55 g dm<sup>-3</sup> zinc and 150 g dm<sup>-3</sup> sulfuric acid solution was prepared by

(ZnSO<sub>4</sub>·7H<sub>2</sub>O) and analytical grade H<sub>2</sub>SO<sub>4</sub>, and the specific experimental procedures were similar to that described previously [26]. The ionic liquid additive 1-butyl-3-methylimidazolium hydrogen sulfate-[BMIM]HSO<sub>4</sub> was laboratory synthesized, and the specific synthetic methods were mentioned previously [27]. The influence of [BMIM]HSO<sub>4</sub> on the zinc deposition process was analyzed with adding 5 mg dm<sup>-3</sup> of this additive to electrolyte, which was found to be the optimum additive concentration in the previous study [26]. The electrolyte was deoxygenated by bubbling ultrapure argon for at least 10 min prior to each experiment.

Electrochemical studies were based on the analysis of cyclic voltammetry and potentiostatic current-time transients. All the electrochemical measurements were measured by using a GAMRY PCI4/300 electrochemical work station and carried out in a conventional three-electrode electrochemical cell at 40 °C under atmospheric condition with a platinum wire ( $\Phi 1 \times 10 \text{ mm}^2$ ) counter electrode and a saturated calomel electrode (SCE) mounted inside a Luggin capillary as the reference electrode. Before each experiment, the working electrode aluminum disk ( $\Phi 4 \text{ mm}$ ) was ground with 1200 grit silicon carbide paper and polished using 0.5 µm high-purity alumina and then degreased with anhydrous alcohol in an ultrasonic bath for 1 min, washed with doubly distilled water and finally dried.

Cyclic voltammetric experiments were carried out at a constant scan rate of 10 mV s<sup>-1</sup> from the initial potential of -0.70 V to the final potential of -1.25 V. Potentiostatic current-time transients were obtained at a series of constant potentials chosen from the activation controlled region. Bulk zinc deposits were prepared on aluminum disk electrode ( $\Phi 4 \text{ mm}$  diameter, 99.995%). The electrodeposited cathode was removed from the cell and washed thoroughly with distilled water and dried. A Tescan VEGA II XMH microscope was used to examine the surface morphology of the electrodeposits.

## 3 Results and discussion

### 3.1 Cyclic voltammetric studies

The cyclic voltammograms recorded for the major characteristics of the zinc deposition process in the absence and presence of [BMIM]HSO<sub>4</sub> as additive are depicted in Fig. 1. The voltammograms were initiated at point 'A' (-0.70 V), scanned in the negative direction and reversed at point 'C' (-1.25 V) in the positive direction. The cathodic current increased sharply once zinc electroreduction began at point 'B' (ca. -1.16 V), followed by a current loop as the direction of sweeping was reversed. This reversed scanning resulted in a decrease in current

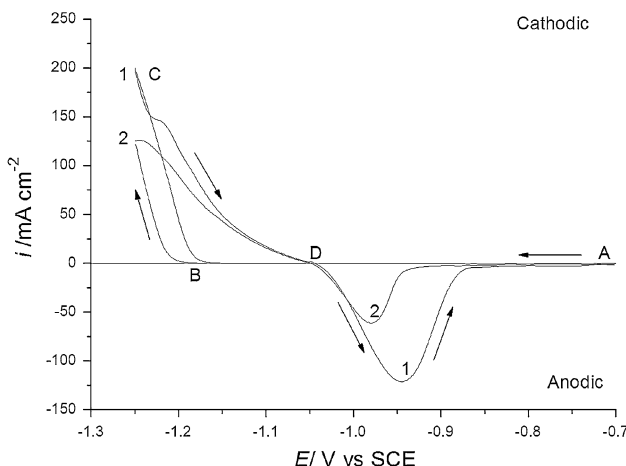


**Fig. 1** Cyclic voltammograms of acidic zinc sulfate solutions in the presence of  $[{\text{BMIM}}]\text{HSO}_4$ . (1) Blank, (2)  $5 \text{ mg dm}^{-3}$   $[{\text{BMIM}}]\text{HSO}_4$

which subsequently reached zero at the crossover potential, ‘D’ (ca.  $-1.05 \text{ V}$ ) and the current then became anodic corresponding to the dissolution of the deposited zinc previously formed. The appearance of such hysteresis loop is a characteristic feature of a nucleation and growth process [28]. In this case, an overpotential is required to form the first nuclei on the substrate surface and the afterward increase in the current density is due to the growth of the first nuclei [17]. The potential difference between the electroreduction potential of zinc ion and the crossover potential is a measure of nucleation overpotential (NOP) for zinc deposition on an aluminum substrate. It is clear that the addition of  $[{\text{BMIM}}]\text{HSO}_4$  shifts the maximum of the cathodic peak corresponding to the  $\text{Zn}^{2+}$  reduction toward more negative value (increased the ‘NOP’ value), along with the reduction of cathodic process area, denoting an inhibition of the electrocrystallization. This is generally attributed to the surface coverage of the cathode by a strongly adsorbed additive layer, which increases the interfacial viscosity, decreases the mass transfer, and slows the deposition rate. Therefore, additional energy is required to discharge the metal ions, and consequently, the deposition overpotential is increased.

### 3.2 Chronoamperometric analysis

Chronoamperometry measurements were carried out to investigate the zinc nucleation/growth process in more detail. These experiments were performed at different overpotentials during zinc electrodeposition on aluminum from acidic sulfate solution in the absence and presence of  $[{\text{BMIM}}]\text{HSO}_4$ . The shape of the current transients is typical of diffusion-limited nucleation process with three-dimensional growth of a metal on a foreign metal substrate [29] and shown in Fig. 2. The initial increase in the current

observed at the first short time is corresponding to an increase in the electroactive area as independent nuclei grows and/or the number of nuclei increases. At later stages, the diffusion zones of the growing adjacent nuclei overlap and the rising current eventually terminates in a broad maximum ( $i_m$ ) followed by a decaying portion, converging to a limiting current approaching the limiting form for linear diffusion of the electroactive ions to a planar electrode, i.e., the Cottrell equation [29]:

$$I = nFSc(D/\pi)^{1/2}t^{-1/2} \quad (1)$$

where  $S$  represents the electrode area,  $D$  is the diffusion coefficient,  $n$  and  $F$  are the number of electrons and Faraday’s constant, respectively,  $c$  is the metal ion bulk concentration, and all other symbols have their usual meaning. The fluctuations in the decaying portion observed in the  $i-t$  curve are due to the hydrogen evolution along with the nucleation process. The values of the maximum current density,  $i_m$  and the time of the maximum current density,  $t_m$  as a function of overpotential,  $\eta$  that are taken from the

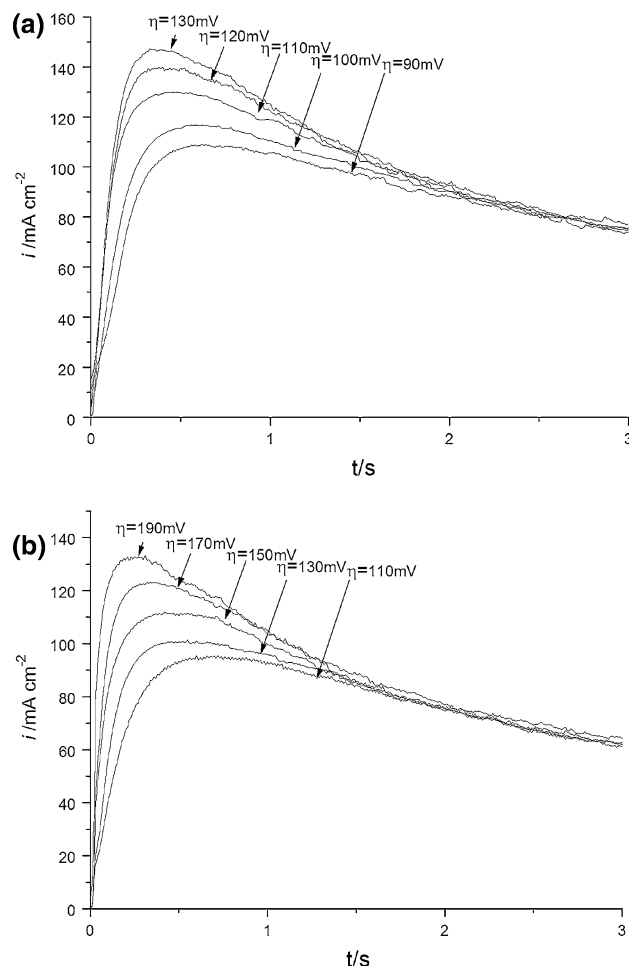


**Fig. 2** Current transient curves in the presence of  $[{\text{BMIM}}]\text{HSO}_4$  at different overpotential. **a** Blank, **b**  $5 \text{ mg dm}^{-3}$   $[{\text{BMIM}}]\text{HSO}_4$

**Table 1** Kinetic parameters extracted from the current density transients for zinc nucleation on aluminum electrode from the solution without additive

$\eta$ (mV)	$t_m$ (s)	$i_m$ (mA cm $^{-2}$ )	$10^4 i_m^2 t_m$ (A $^2$ s cm $^{-4}$ )	$10^6 D$ (cm $^2$ s $^{-1}$ )	$10^{-6} N$ (cm $^{-2}$ )	A (s $^{-1}$ )
90	0.62	108.99	73.65	1.70	0.87	24.55
100	0.59	115.74	73.68	1.70	0.97	31.62
110	0.46	129.92	77.64	1.79	1.11	38.21
120	0.40	139.76	78.13	1.80	1.26	46.39
130	0.36	147.37	78.18	1.80	1.40	56.84

**Table 2** Kinetic parameters extracted from the current density transients for zinc nucleation on aluminum electrode from the solution containing 5 mg dm $^{-3}$  [BMIM]HSO $_4$ 

$\eta$ (mV)	$t_m$ (s)	$i_m$ (mA cm $^{-2}$ )	$10^4 i_m^2 t_m$ (A $^2$ s cm $^{-4}$ )	$10^6 D$ (cm $^2$ s $^{-1}$ )	$10^{-6} N$ (cm $^{-2}$ )	A (s $^{-1}$ )
110	0.60	95.58	54.81	1.26	1.20	30.64
120	0.55	101.34	53.40	1.23	1.42	38.16
130	0.42	111.99	52.68	1.21	1.79	46.67
140	0.36	123.09	54.54	1.25	2.01	57.80
150	0.31	132.79	54.66	1.26	2.33	70.50

current–time transients resulting from a typical experiment are presented in Tables 1 and 2. It is observed that the time at which  $i_m$  occurs,  $t_m$  depends on the applied overpotential,  $\eta = |E - E_{eq}|$ . Examination of the data in these Tables reveals that, as expected,  $i_m$  increases and  $t_m$  decreases as  $\eta$  is increased. In addition, a higher overpotential value is required to initiate the nucleation and subsequent growth of the zinc deposits with the addition of [BMIM]HSO $_4$ . These results are associated with the adsorption of the additive on the substrate surface, leading to decrease in the nucleation and growth rate of the zinc ions [17]. Therefore, the higher overpotentials are needed to obtain a current maximum in the potentiostatic transients in the solution containing [BMIM]HSO $_4$ .

Several models have been developed to describe the diffusion controlled growth nucleation process. Two limiting cases can be observed: instantaneous nucleation, where all nuclei are formed immediately after the potential step; and progressive nucleation, where the number of nuclei increases during the whole deposition process. An excellent method for discriminating between these two limiting nucleation and growth models was proposed by Sharifker and Hills [29]. A more definitive test for adherence to the two models can be made by comparing data from the entire experimental current–time transient to the appropriate dimensionless theoretical equation derived on the basis of the models. The expressions given in Eqs. 2 and 3 relate the dimensionless current to the dimensionless time for diffusion controlled three-dimensional instantaneous and progressive nucleation and growth, respectively. The resulting expressions for these quantities for both cases are given in Table 3.

**Table 3** Expressions resulting from the analysis of the current maxima for 3D instantaneous and progressive nucleation*Instantaneous nucleation*

$$t_m = \frac{1.2564}{N_0 \pi k D} \quad (a)$$

$$i_m = 0.6382 z F D c (k N_0)^{1/2} \quad (b)$$

$$i_m^2 t_m = 0.1629 (z F c)^2 D \quad (c)$$

$$\left(\frac{i}{i_m}\right)^2 = 1.9542 \left\{1 - \exp\left[-1.2564 \left(\frac{t}{t_m}\right)\right]\right\}^2 \left(\frac{t}{t_m}\right)^{-1} \quad (d)$$

*Progressive nucleation*

$$t_m = \left(\frac{4.6733}{A N_\infty \pi k' D}\right)^{1/2} \quad (e)$$

$$i_m = 0.4615 z F D^{3/4} c (k' A N_\infty)^{1/4} \quad (f)$$

$$i_m^2 t_m = 0.2598 (z F c)^2 D \quad (g)$$

$$\left(\frac{i}{i_m}\right)^2 = 1.2254 \left\{1 - \exp\left[-2.3367 \left(\frac{t}{t_m}\right)^2\right]\right\}^2 \left(\frac{t}{t_m}\right)^{-1} \quad (h)$$

$$(i/i_m)^2 = 1.9542 \left\{1 - \exp\left[-1.2564 \left(\frac{t}{t_m}\right)\right]\right\}^2 \left(\frac{t}{t_m}\right)^{-1} \quad (2)$$

$$(i/i_m)^2 = 1.2254 \left\{1 - \exp\left[-2.3367 \left(\frac{t}{t_m}\right)^2\right]\right\}^2 \left(\frac{t}{t_m}\right)^{-1} \quad (3)$$

In Fig. 3, the experimental dimensionless current–time transients compared to the theoretical transients were calculated from Eqs. 2 and 3. From this Figure, it is apparent that the experimental data is in excellent agreement with the limiting model for instantaneous nucleation, indicating that the electrocrystallization occurred by 3D instantaneous nucleation on the active sites with nuclei growing at the diffusion-limited rate. The transients obtained from the solution in the presence of 5 mg dm $^{-3}$  [BMIM]HSO $_4$  are

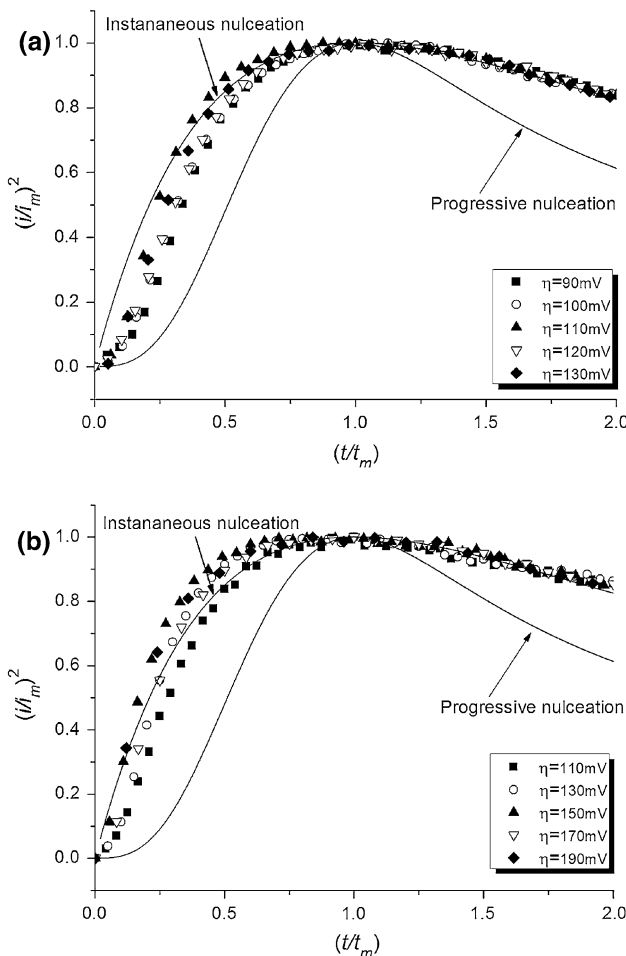


**Fig. 3** Comparison of the dimensionless experimental data derived from the current transients with theoretical models for diffusion controlled 3D instantaneous and progressive nucleation. **a** Blank, **b** 5 mg dm<sup>-3</sup> [BMIM]HSO<sub>4</sub>

qualitatively similar to the obtained in the absence of the additive, which means that the early stages of the nucleation and growth mechanism for the zinc electrodeposition process is not changed with the addition of this additive. The major difference is that the higher overpotential value is required to initiate the nucleation and subsequent growth of the zinc deposits, which is in agreement with the cyclic voltammetric results.

These transients could be used to determine several nucleation parameters, such as the diffusion coefficient of the electroactive species,  $D$ ; the number density of active sites,  $N$ ; and nucleation rate per site,  $A$ . Although the two models mentioned above are widely used to discuss the progressive or instantaneous character of reactions, in practice it is difficult to extract useful parameters from them [30]. A model proposed by Sharifker and Mostany [31] provides a new route to estimate the kinetic parameters without necessary to classify the nucleation process.

The nucleation parameters  $N$  and  $A$  can be obtained separately from the current density maximum recorded during an experimental transient using Eq. 4:

$$i(t) = \left( \frac{zFD^{1/2}c}{\pi^{1/2}t^{1/2}} \right) \left\{ 1 - \exp \left[ -N\pi k^* D \left( t - \frac{1 - e^{-At}}{A} \right) \right] \right\} \quad (4)$$

where  $k^* = (8\pi cM/\rho)^{1/2}$ ,  $zF$  is the molar charge transferred during electrodeposition,  $D$  is the diffusion coefficient,  $c$  is the metal ion bulk concentration,  $M$  is the molar mass of the deposit, and  $\rho$  is the density of the deposited material.

For this case, the diffusion coefficients for the Zn<sup>2+</sup> ions in both solution conditions, without ( $D_0$ ) and with 5 mg dm<sup>-3</sup> [BMIM]HSO<sub>4</sub> ( $D_B$ ), could be calculated separately by linearization of the falling part of the transients for long time according to the Cottrell equation. The corresponding values are  $D_0 = 1.76 \times 10^{-6}$  cm<sup>2</sup> s<sup>-1</sup> and  $D_B = 1.24 \times 10^{-6}$  cm<sup>2</sup> s<sup>-1</sup>. These parameters were used for the evaluation of the  $N$  and  $A$  values. Figure 4 shows a comparison of the

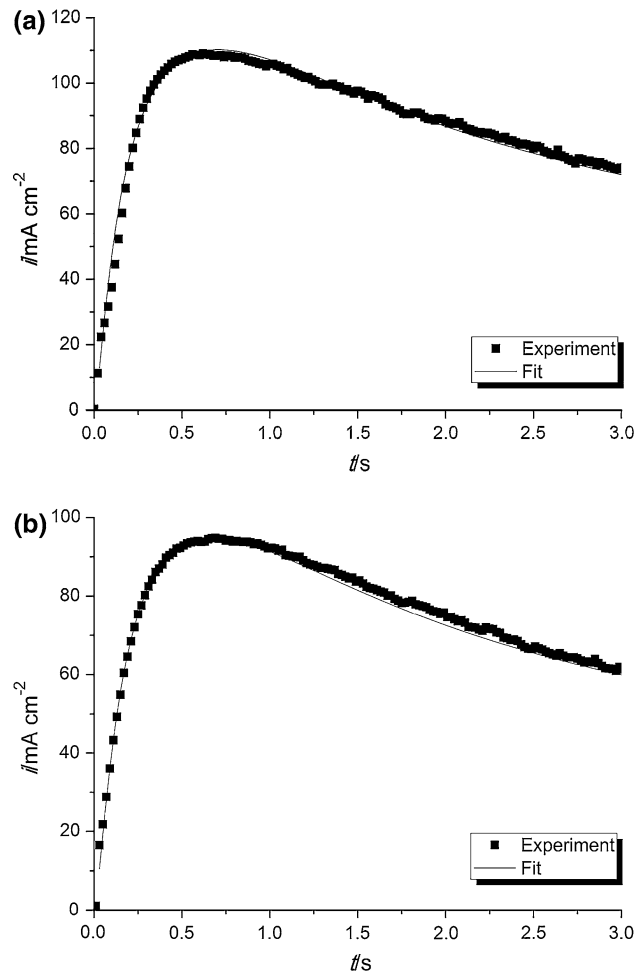


**Fig. 4** Fitting the dimensionless experimental data derived from the current transients using Eq. 4. **a** blank,  $\eta = 90$  mV, **b** 5 mg dm<sup>-3</sup> [BMIM]HSO<sub>4</sub>,  $\eta = 110$  mV

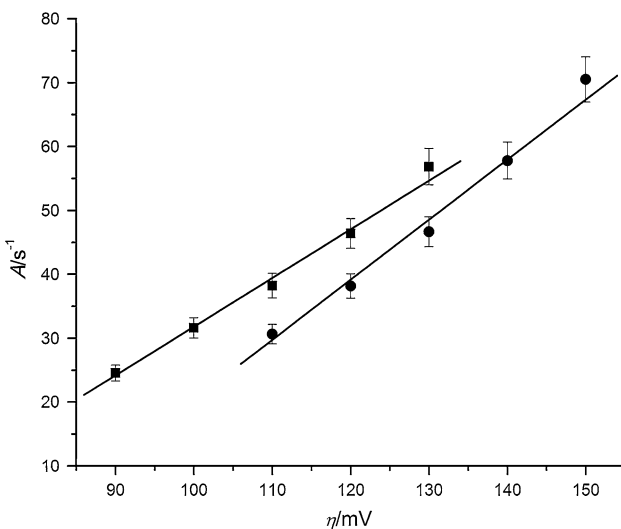


**Fig. 5** Overpotential dependence of the nucleation rate constant,  $A$ . *filled square* Blank, *filled circle*  $5 \text{ mg dm}^{-3}$  [BMIM]HSO<sub>4</sub>. The error bars indicate the percentage error of each determination

experimental transient obtained at  $\eta = 90 \text{ mV}$  in the absence of additive (Fig. 4a) and at  $\eta = 110 \text{ mV}$  with  $5 \text{ mg dm}^{-3}$  [BMIM]HSO<sub>4</sub> (Fig. 4b), respectively, during electrodeposition of zinc onto aluminum and the current-time transient generated by non-linear fitting using Eq. 4 to the experimental data. During the fitting process, the parameters  $N$  and  $A$  were obtained and given in Tables 1 and 2.

By comparison the results obtained, it could be concluded that the presence of [BMIM]HSO<sub>4</sub> in the solution decreases the nucleation and growth rate as higher overpotentials are needed to obtain a current maximum in the potentiostatic transients. As shown in Fig. 5, the dependence of  $A$  with the overpotential  $\eta$  could be interpreted on the basis of the atomistic theory of electrolytic nucleation [32–34]. According to this theory, the nucleation rate constant,  $A$ , is given by [25, 32].

$$A = k^+ \exp\left[\frac{-\phi(n_k)}{kT}\right] \exp\left[\frac{(n_k + \beta)ze\eta}{kT}\right] \quad (5)$$

where  $k^+$  is the frequency factor,  $\beta$  is the transition coefficient,  $n_k$  the number of atoms in the critical nucleus and  $\phi(n_k)$  accounts for the nucleus–substrate interaction. Therefore,  $n_k$  can be obtained using follows equation:

$$n_k = \left(\frac{2.303RT}{zF}\right) \left(\frac{d \log A}{d \eta}\right) \quad (6)$$

From the slope of the straight lines in Fig. 5, then Eq. 6 gives  $n_k \approx 0.3$  in both cases, in the absence and presence of  $5 \text{ mg dm}^{-3}$  [BMIM]HSO<sub>4</sub> in the electrolyte. The values of  $n_k$  ranging from 0 to 1 were observed for the electrodeposition of copper [35], cadmium [36], lead [37], and silver [38] on GC in aqueous solutions, which indicated that active sites on the electrode surface probably act as the

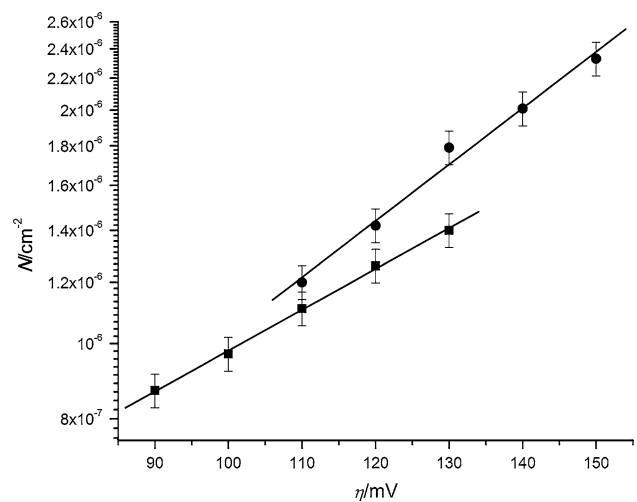


**Fig. 6** Overpotential dependence of the number density of nucleus,  $N$ . *filled square* Blank, *filled circle*  $5 \text{ mg dm}^{-3}$  [BMIM]HSO<sub>4</sub>. The error bars indicate the percentage error of each determination

critical nucleus [32] during the electrodeposition of zinc. This analysis may be inferred that the addition of [BMIM]HSO<sub>4</sub> does not drastically change the size of the critical nucleus at the initial stages. The decrease in the nucleation rate in the presence of [BMIM]HSO<sub>4</sub> could be associated with the blocking effect of the adsorbed additive, resulting in a decrease in the rate of the ions transferred across the electric double layer [39].

Concerning the number density of active sites, the variation of  $N$  as a function of applied overpotential is shown in Fig. 6.  $N$  varies exponentially linearly with applied overpotential. Table 1 shows practically no variations of  $N$  with the overpotential for the nucleation of Zn onto aluminum electrode from the solution without additive at a relatively high nucleation rate. The nucleation seems to be attributed to a low number of active sites on the surface which become exhausted at the original stage of the process. The process is consistent with the instantaneous nucleation predicted previously. Similar observation is obtained in the presence of  $5 \text{ mg dm}^{-3}$  [BMIM]HSO<sub>4</sub> (Table 2), however, the  $N$  value is found to be higher than that of additive-free solution at a given potential, indicating the additive induce an increase in the number of the nuclei formed. This behavior may be attributed to the contribution of the additive on the existence of a distribution of site energies on the surface. As the cathodic overpotential increases, a larger fraction of sites become active [40].

### 3.3 Morphological studies

The morphology of zinc electrodeposits on aluminum from acidic sulfate solution was analyzed by SEM to determine

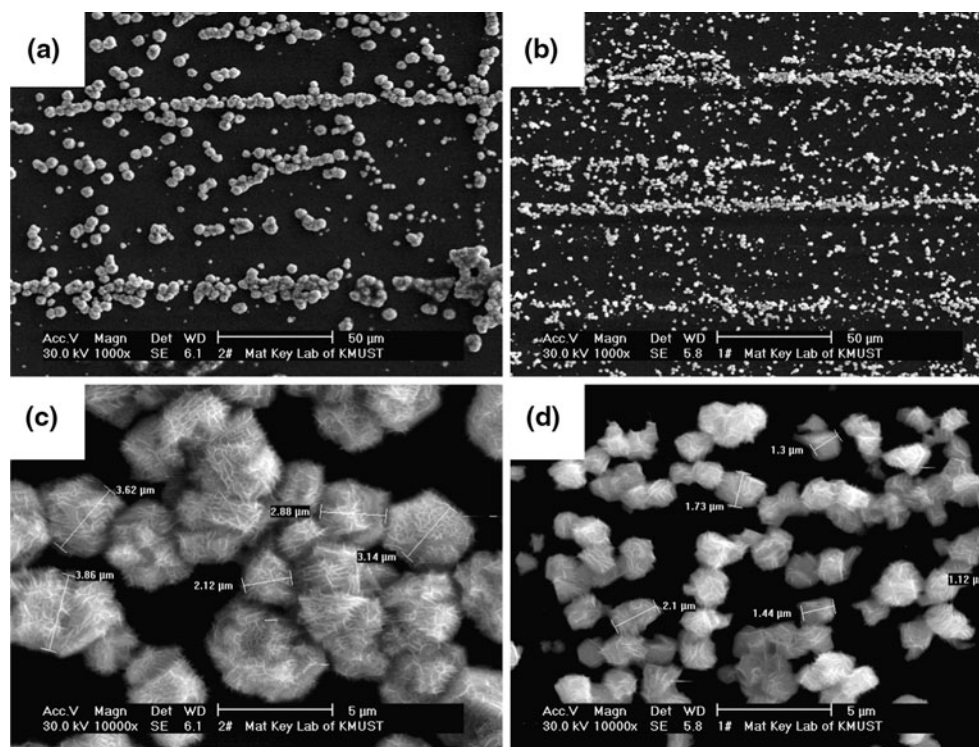


**Fig. 7** SEM micrographs of the zinc deposits in the absence ( $\eta = 90$  mV,  $t = 60$  s) and presence of [BMIM]HSO<sub>4</sub> ( $\eta = 120$  mV,  $t = 60$  s). **a, c** Blank, **b, d** 5 mg dm<sup>-3</sup> [BMIM]HSO<sub>4</sub>

the effect of [BMIM]HSO<sub>4</sub> on the initial stages of the deposition process. The deposits were potentiostatically grown at  $\eta = 90$  mV for 60 s in the absence of additive and at  $\eta = 120$  mV for 60 s in the presence of [BMIM]HSO<sub>4</sub>, respectively. In both cases, the Zn deposition occurs preferentially at surface defects or step edges (Fig. 7a, b) which acts as active sites. In the very initial deposition stages of the case in the absence of additive, the deposit obtained is in the form of hemispherical hexagonal plates with similar sizes (Fig. 7c) as is typical for the pure zinc electrodeposits [41, 42], which is in good agreement with the instantaneous nucleation mechanism indicated previously. In the presence of additive, similar result is obtained with a reduction in platelet size (Fig. 7d). The decrease in crystallites size is expected on account for the blocking effect of the additive through cathodic adsorption on the electrode surface that causes a reduction in both the nucleation and growth rate of nuclei, however, the influence on the growth of the nuclei is much more dominant, thus leads to an increase in the number of the nuclei formed and a decrease in the size of these nuclei.

#### 4 Conclusions

The first stages of the zinc electrodeposition process on aluminum electrode from acidic sulfate solutions were

investigated in the absence and presence of [BMIM]HSO<sub>4</sub> as additive. Cyclic voltammetry studies showed the electrodeposition of zinc for both cases were associated with a nucleation and growth process. From the analysis of the corresponding dimensionless chronoamperometric current–time transients, the initial stages of the zinc electrodeposition process could be explained on the basis of a three-dimensional instantaneous nucleation with diffusion controlled growth of the nuclei. The addition of [BMIM]HSO<sub>4</sub> led to decrease the nucleation and growth rate of these nuclei, increase the number density of active sites, and produce cathodic deposits with smaller grain size, however, the instantaneous nucleation mechanism involved for the deposition process was practically unchanged. The result was produced by the blocking effect of [BMIM]HSO<sub>4</sub> on the zinc electrocrystallization process through its cathodic adsorption on the electrode surface.

**Acknowledgments** The authors gratefully acknowledge the financial support of the National Natural Science Foundation of China (Projects no. 50864009 and 50904031) and the Research Fund for the Doctoral Program of Higher Education of China (Project no. 20070674001).

#### References

- Pletcher D (1984) Industrial electrochemistry. Chapman and Hall, London

2. Crotty D (1996) Met Finish 94:54
3. Wilcox GD, Gabe DR (1993) Corros Sci 35:1251
4. Gurmen S, Emre M (2003) Miner Eng 16:559
5. Beshore AC, Flori BJ, Schade G, O'Keefe TJ (1987) J Appl Electrochem 17:765
6. Mackinnon DJ, Brannen JM, Kerby RC (1979) J Appl Electrochem 9:55
7. Mackinnon DJ, Brannen JM, Kerby RC (1979) J Appl Electrochem 9:71
8. Ault AR, Frazer EJ (1988) J Appl Electrochem 18:583
9. Muresan L, Maurin G, Oniciu L, Gaga D (1996) Hydrometallurgy 43:345
10. Robinson DJ, O'Keefe TJ (1976) J Appl Electrochem 6:1
11. MacKinnon DJ, Brannen JM (1977) J Appl Electrochem 7:451
12. Lamping BA, O'Keefe TJ (1976) Metall Trans 7B:551
13. Oniciu L, Muresan L (1991) J Appl Electrochem 21:565
14. MacKinnon DJ, Brannen JM (1982) J Appl Electrochem 12:21
15. Michailova E, Peykova M, Stoychev D, Milchev A (1994) J Electroanal Chem 366:195
16. Budevski E, Staikov G, Lorenz WJ (1996) Electrochemical phase formation and growth. VCH, New York
17. Trejo G, Ruiz H, Ortega R, Meas Y (2001) J Appl Electrochem 31:685
18. Trejo G, Ortega R, Meas Y (2002) Plat Surf Finish 89:84
19. Yu J, Wang L, Su L, Ai X, Yang H (2003) J Electrochem Soc 150:C19
20. Higashi K, Fukushima H, Urawaka T, Adaniya T, Matsudo K (1981) J Electrochem Soc 128:2081
21. Baldwin KR, Smith CJ, Robinson MJ (1994) Trans Inst Met Finish 72:79
22. Tsuru T, Kobayashi S, Akiyama T, Fukushima H, Gogia SK, Kammel R (1997) J Appl Electrochem 27:209
23. Sonneveld PJ, Visscher W, Barendrecht E (1992) Electrochim Acta 37:1199
24. Raeissi K, Saatchi A, Golozar MA (2003) J Appl Electrochem 33:635
25. Alvarez AE, Salinas DR (2004) J Electroanal Chem 566:393
26. Zhang QB, Hua YX (2009) J Appl Electrochem 39:261
27. Whitehead JA, Lawrence GA, McCluskey A (2004) Aust J Chem 57:151
28. Fletcher S (1983) Electrochim Acta 28:917
29. Scharifker BR, Hills G (1983) Electrochim Acta 28:879
30. Hyde ME, Compton R (2003) J Electroanal Chem 549:1
31. Scharifker BR, Mostany J (1984) J Electroanal Chem 177:13
32. Milchev A, Stoyanov S, Kaischev R (1974) Thin Solid Films 22:255
33. Milchev A, Stoyanov S (1976) J Electroanal Chem 72:33
34. Milchev A, Tsakova V (1990) J Appl Electrochem 20:301
35. Gunawardena G, Hills G, Montenegro I (1985) J Electroanal Chem 184:357
36. Gunawardena G, Hills G, Montenegro I (1985) J Electroanal Chem 184:371
37. Mostany J, Parra J, Scharifker BR (1986) J Appl Electrochem 16:333
38. Gunawardena G, Hills G, Montenegro I (1982) J Electroanal Chem 138:241
39. Michailova E, Vitanova I, Stoychev D, Milchev A (1993) Electrochim Acta 38:2455
40. Deutscher RL, Fletcher S (1988) J Electroanal Chem 235:17
41. Barceló G, Sarret M, Müller C, Pregonas J (1998) Electrochim Acta 43:13
42. Yan H, Downes J, Boden PJ, Harris SJ (1996) J Electrochem Soc 143:1577